ACS ES&T Air

pubs.acs.org/estair

Article

Characterizing Atmospheric Emissions of Particulate Matter from Copper Smelting through Coriolis-μ Air Sampling and Single Particle ICP−MS Analysis

Aaron J. Goodman,* Houssame-Eddine Ahabchane, Patrick L. Hayes, and Kevin J. Wilkinson*

Cite This: https://doi.org/10.1021/acsestair.5c00307

Read Online

ACCESS | Metrics & More | Article Recommendations | Supporting Information

ABSTRACT: New methods of air sampling and analysis are needed to better understand atmospheric emissions from industrial sources. To close this knowledge gap, 80 air samples were collected around a copper smelter in Quebec using a Coriolis-μ device, allowing for rapid, spatially and temporally resolved samples. Airborne particles were collected directly into water allowing for (a) precise total elemental quantification by inductively coupled plasma mass spectrometry (ICP−MS) following acidification and (b) analysis of individual particle compositions by single particle ICP-Time-of-Flight-MS (spICP-ToF-MS). This new combination of sampling and analytical techniques allowed for better interpretation of the timing, magnitude and elemental signature of emissions from the smelter. Orders-of-magnitude changes in elemental concentrations including As, Pb, and Cd occurred on time scales as short as 15 min, as revealed by high resolution sampling. Furthermore, strong correlations were observed in both bulk elemental concentrations and particle number concentrations (PNCs) among chalcophile elements, including Cu, As, Cd, and Pb. Distance transect sampling further demonstrated the utility of the Coriolis, with 12 sites sampled on a single day. The downwind persistence of airborne metal(loid)s was measured as far as 6 km from the smelter. The coupling of Coriolis sampling with spICP-ToF-MS analysis provided further insights into emission sources of the submicron particles. A consistent proportion of As- and Pb-bearing particles with respect to co-occurring major elements was observed over time, even as PNCs varied by up to 66-fold; this suggested a single source responsible for the majority of the particles. The multielement particle signatures, including In and Sn present with As, Sb, and/or Bi, and a lack of Cu in many of the trace element particles suggested a smelting origin.

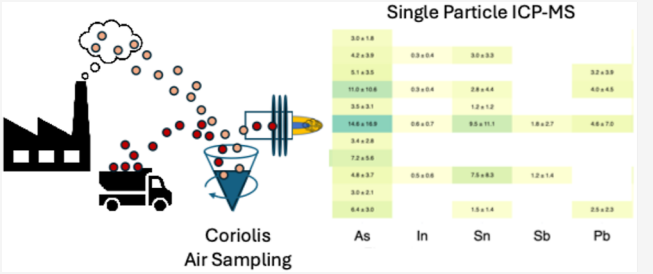

KEYWORDS: *metal aerosols, particulate matter, nanoparticles, single particle ICP-ToF-MS, copper smelting*

Downloaded via Aaron Goodman on January 13, 2026 at 21:43:12 (UTC).
See https://pubs.acs.org/sharingguidelines for options on how to legitimately share published articles.

1. INTRODUCTION

Atmospheric emissions of particulate matter (PM) have long been a concern for environmental and public health. Industrial processes, including mining and smelting, contribute a large fraction of global anthropogenic emissions.[1,2] Nonferrous metal smelters, which are designed to process Cu, Pb or Zn ores can emit As, Pb, Cd, Tl in significant quantities to the atmosphere in the form of aerosols.[3] The particulate forms of these metal(loid)s are potentially toxic to both humans and aquatic life. Sulfur dioxide (SO_2) is emitted from this process via oxidation of sulfide minerals, but is largely collected and converted to sulfuric acid. To facilitate a transition toward carbon-neutral energy sources, the demand for critical raw materials including Cu is increasing.[4] A global depletion of high-grade ores will require smelters to handle concentrates with greater concentrations of impurities.[5] Moreover, smelters are processing increased loads of recycled electronics, which likely contain different impurity elements compared with ores. Therefore, a better understanding of emissions from mining and smelting is needed to protect human health and the environment. There are many possible sources of particulate emissions from smelters, including, but not limited to copper concentrate feedstock, recycled copper feedstock, dust associated with feedstock transport, slag, condensate particles formed from metal(loid)s volatilized during smelting, and any combinations thereof. Thus, analytical advancements are also required to better constrain these emission sources.

The monitoring of particulate emissions from smelters is typically performed by trapping airborne particles on a filter. These filter samplers can be equipped with impactors to enable the capture of PM with specific particle diameters, e.g. <10 μm (PM_{10}) or <2.5 μm ($PM_{2.5}$). The filter is then analyzed by techniques such as X-ray fluorescence (XRF) or microscopic techniques such as scanning electron microscopy coupled with

Received: August 4, 2025
Revised: January 7, 2026
Accepted: January 8, 2026

© XXXX American Chemical Society

energy dispersive spectroscopy (SEM/EDS) in order to obtain total elemental concentrations. Alternatively, filters can be digested prior to measurement by inductively coupled plasma mass spectrometry (ICP−MS).

There are several limitations to filter-based air quality monitoring. Filters are typically collected and analyzed every 24−48 h, providing average concentrations, despite emissions generally being transient phenomena. The systems used to monitor air are often permanent or semipermanent installations, limiting spatially resolved monitoring capability. For SEM/EDS analysis, the number of analyzed particles is often low, and elemental composition often cannot be determined in particles <1 μm. Advances including automated systems for particle composition analysis (e.g., TIMA, QEMSCAN) and time-resolved XRF based systems might alleviate some of these issues, however, the single particle analysis of submicron sized aerosols is still difficult, especially for short-term emissions lasting <1 h. This is especially important given the differences between mass and number distributions and the dependence of associated human health impacts on particle size (i.e., a single large particle may represent the same mass of many small particles but pose a much lower risk). To accurately predict human health outcomes due to the atmospheric emission of particles, it is necessary to precisely measure particle concentrations, chemical compositions and sizes.

This study demonstrates advances in air sampling and analysis that provide solutions to address some of these issues. First, high-frequency sampling of aerosols was performed using a portable Coriolis-μ device (referred to as a Coriolis). PM was collected in Milli-Q water and samples could be readily analyzed by ICP−MS after acidification with nitric acid. Single particle inductively coupled plasma time-of-flight mass spectrometry (spICP-ToF-MS) was also employed to analyze the composition of individual submicron particles sampled with the Coriolis. This high-throughput approach for characterization of small (ca. ≥ 50−100 nm) individual particles is especially important given the increased toxicological impacts of the fine and ultrafine particles.[6] spICP-ToF-MS has recently been applied to the study of inorganic aerosols collected on filters.[7,8]

We demonstrate these advances in air sampling and analysis through a study of air quality surrounding a smelter in Quebec. Emission of SO_2, PM, and metal(loid)s including As, Cd, and Pb have long been a concern for the surrounding communities.[9] Despite recent progress to reduce emissions, the levels of many metal(loid)s are still a concern to the local community. By collecting air samples at high time resolution and by analyzing both total elemental concentrations and the composition of individual particles, we gain new insights into the timing, magnitude and sources of the transient emissions.

2. METHODS AND MATERIALS

2.1. High Resolution Sampling of Aerosols

The Coriolis air sampler operates by vortexing air through a HDPE cone filled with ultrapure water, such that the airborne particles are pulled into the water and remain suspended as the air is cycled through the cone. In our setup, the Coriolis was operated at a flow rate of 300 L min^{-1} for a duration of 6 min per sample. All cones were acid washed prior to the sampling campaigns and were field rinsed using Milli-Q water immediately prior to sampling. For time-resolved sample sets, the same cone was used and was triple rinsed with Milli-Q water between samples. For distance-based samples, a new cone was used at each site. For all samples, 15 mL of Milli-Q water was predispensed into polyethylene tubes (Falcon), then poured into a rinsed sampling cone in the field. Differences in temperature and relative humidity led to variable evaporative losses during sampling. To account for this, the lost water was replaced by Milli-Q water in the field in order to maintain constant volume.

2.2. Field Sampling

Two sampling campaigns were conducted in Quebec, Canada in October and November 2024. During the October campaign, one series of 24 samples (A: time) was collected on the roof of an office located about 500 m south of the entrance of the smelter complex. The Coriolis sampler was placed on top of a wooden box approximately 1 m above the roof. Samples of a 6 min duration were collected every 15 min (with 9 min between samples). During the November sampling campaign, a second set of 25 samples (B: time) was collected at 6 min intervals. The Coriolis was placed on a 1 m table, on top of a ∼10 m hill adjacent to the smelter air monitoring station. A third sample set (D: distance) was collected along a distance transect, where 30 samples were collected at 12 sites spaced 0.5−1 km apart along a southwest-northeast route. The line of sampling was oriented along the direction of the wind on the day of sampling in order to collect air both upwind and downwind of the smelter complex. Duplicate samples were collected at all sites, except site D7, immediately downwind of the smelter, where 8 samples were collected due to a highly visible emission event. At all sites, the Coriolis was placed on top of a vehicle, resulting in an inlet height of ∼1.5 m above ground. Sample locations relative to the smelter complex are displayed in Figure 1 and described in Table 1.

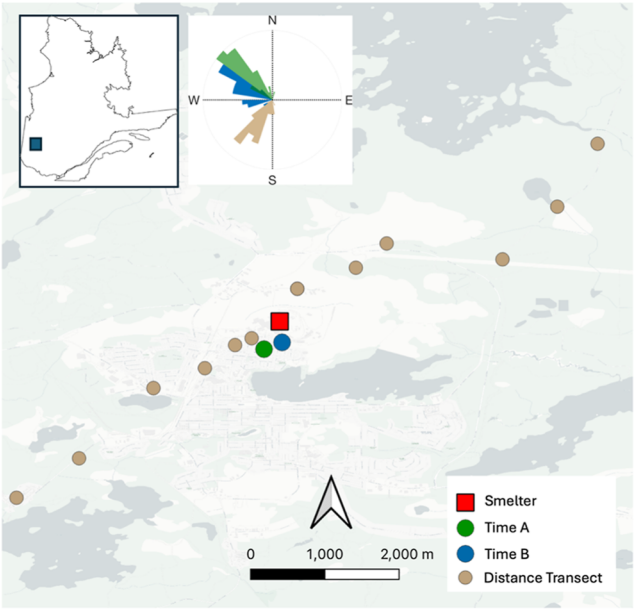

Figure 1. Map of the region, including the location of the Cu smelter (location within Quebec shown in one inset, winds on the day of sampling shown in the second inset), the two time-resolved sample sets and the distance transect.

For sample sets A and D, samples were returned to the laboratory at the University of Montreal, vortexed, sonicated in an ultrasonic bath, then split into two subsamples for analysis of total metal(loid)s (using ICP−MS) and single particles (using spICP-ToF-MS). The total metal(loid)s subsamples were acidified to 2% using ultrapure nitric acid (SCP science). For sample set B, samples from the sampling cone were divided into subsamples in the field; one was acidified for bulk analysis, and the unacidified sample was analyzed by spICP-ToF-MS following its ultrasonication for 10 min and dilution in MQW (between 5 and 50-fold).

https://doi.org/10.1021/acsestair.5c00307
ACS EST Air XXXX, XXX, XXX−XXX

Table 1. Sample IDs, Coordinates, Distance from Smelter, and Surrounding Environment for Each Sample.[a]

sample/Site ID	lat	long	distance from smelter (km)	sample number/type	environment
A1−A24	48.2484	−79.0159	0.51	24	roof
B1−B25	48.2496	−79.0127	0.44	25	grass hill
D1	48.2215	−79.0608	−4.80	2	low traffic street
D2	48.2286	−79.0494	−3.65	2	off highway
D3	48.2413	−79.0360	−1.94	2	parking lot
D4	48.2449	−79.0266	−1.17	2	parking lot
D5	48.2491	−79.0212	−0.55	2	low traffic street
D6	48.2503	−79.0182	−0.32	2	low traffic street
D7	48.2593	−79.0099	0.85	8	industrial road
D8	48.2631	−78.9993	1.69	2	golf course
D9	48.2675	−78.9937	2.32	2	gravel road
D10	48.2646	−78.9727	3.47	2	dirt road
D11	48.2741	−78.9628	4.60	2	dirt road
D12	48.2855	−78.9555	5.77	2	dirt road
monitoring station	48.2496	−79.0127	0.44	XRF,SO_2	--
P4	48.234447	−78.9993	2.44	SO_2	--

[a]Negative distance indicates upwind, positive indicates downwind. Sample number refers to number of samples taken at each site. XRF refers to metal(loid) concentrations analyzed by the Xact X-ray fluorescence (XRF) system.

2.3. ICP−MS Analyses

The acidified subsamples were analyzed for 22 elements using a PerkinElmer NexION 5000 mass spectrometer, equipped with a glass cyclonic spray chamber and a concentric nebulizer. Isotopes were chosen to maximize abundance (sensitivity) and minimize interferences: ^{27}Al, ^{28}Si, ^{48}Ti, ^{52}Cr, ^{55}Mn, ^{57}Fe, ^{59}Co, ^{60}Ni, ^{63}Cu, ^{65}Cu, ^{66}Zn, ^{75}As, ^{107}Ag, ^{111}Cd, ^{115}In, ^{118}Sn, ^{121}Sb, ^{128}Te, ^{139}La, ^{140}Ce, ^{205}Tl, ^{206}Pb, ^{207}Pb, ^{208}Pb and ^{209}Bi. As, Fe, Si and Cr were analyzed in mass-shift mode with an oxygen flow rate of 0.7 mL min. Calibration standards of 0.1, 1, 10, and 20 μg L^{-1} were prepared from 10 mg L^{-1} stock solutions in 2% ultrapure nitric acid. Terbium was added as an internal standard at 1 μg L^{-1} to correct for matrix effects and changes in instrument sensitivity during analysis. A reference solution of 0.2 μg L^{-1} Co, In, Ce, and Pb was analyzed routinely to monitor performance (recoveries were between 80 and 120%). Despite the short sampling duration, detection limits for total metal(loids) were low, ranging from 10 s of ng m^{-3} for elements with high natural abundance, to <1 ng m^{-3} for trace elements (Table S1).

The unacidified subsamples were analyzed using an ICP-ToF-MS operated in single particle mode (Nu instruments Vitesse, Wrexham, UK). The ICP-ToF-MS acquires data for multiple isotopes quasi-simultaneously; we collected data from m/z 22 to 238, with m/z 30−40 "blanked" to protect the detector from Ar^+ ions.[10] A hydrogen−helium gas mixture was used in the reaction cell to minimize polyatomic species. The dwell time was 80 μs, and the data acquisition time ranged between 3 and 9 min in order to analyze statistically relevant particle numbers. The same aqueous standards described above were used to determine instrument sensitivity. The transport efficiency was determined with 50 and 100 nm Au nanoparticles (NanoComposix) using the mass-based approach.[11] Raw data were processed using the SPCal software.[12] The particle detection threshold was set using the compound-poisson distribution with the false positive rate set at 1×10^{-5} and a two-point minimum detection criteria (i.e., two consecutive dwell times must be greater than the threshold to be considered a peak). The number of particles detected in each sample was corrected for the dilution factor, transport efficiency, and sample uptake rate in order to determine the particle concentration in the Milli-Q water, which was then divided by the volume of air sampled by the Coriolis to calculate the particle number concentration (PNC, particles m^{-3}). The total mass of the particles detected for each element was summed and corrected by the same parameters to determine the total particulate concentration (ng m^{-3}). The baseline signal in the spICP-ToF-MS measurement (primarily dissolved species) was quantified using aqueous calibration standards.

2.4. In Situ Atmospheric Chemistry Analysis

The smelter operator monitors local SO_2, PM, and elemental concentrations using a variety of instrumentation. A SCI Xact 625i located at a monitoring station just outside the smelter gate provides airborne metal(loid) concentrations every hour. The Xact uses a PM_{10} impactor coupled with a reel-to-reel filter tape, which automatically moves to expose fresh tape to the air jet. After the PM is collected, it is analyzed by energy dispersive X-ray fluorescence (ED-XRF) spectroscopy. SO_2 is monitored at the monitoring station and several additional locations around the city, using a Thermo 43*i* SO_2 analyzer based upon ultraviolet emission.

2.5. Methodological Limitations

The primary goal of this study was to apply new sampling and analytical strategies to the study of smelting emissions. Given the potential impact of these and future results on the interpretation of emission sources and comparison to legal air quality standards and human health, it is important to clearly outline current limitations.

The main limitations of the Coriolis sampler are poorly defined size limits for particle capture, and uncertainty in the flow rate. While collection efficiency has been reported to be 92% for 10 μm particles,[13] for the submicron particle sizes that are the most interesting here, adsorptive losses between the plastic cone and the particles could be occurring. The flow rate is stated to be 300 L min^{-1}, but this value is factory calibrated and could not readily be validated in the lab or field. Experiments with multiple samplers, and comparisons to conventional PM10 and PM2.5 filter samplers are ongoing to define these parameters but are outside the scope of the current study.

Bulk elemental concentrations were measured from air samples that were collected in water and acidified to 2% v/v HNO_3. This is a common strategy for analyzing water samples, where particles are assumed to be dissolved prior to analysis. However, some mineral particles might not be soluble in this matrix, which could result in an under-reporting of the total elemental concentrations. Ongoing sampling campaigns have employed strong acid digestions at elevated temperatures to remedy this issue.

There are several limitations to spICP-ToF-MS analysis which are relevant to the results presented here, the most important of which are the estimation of particle sizes measured by the technique, and the size-dependence of the measurement itself. Although ICP−MS quantifies elements from the majority of the periodic table, common low m/z elements including carbon, oxygen, and sulfur that are likely to be present in smelter-associated particles (e.g., sulfides, sulfates, oxides, and black carbon) have extremely poor detection limits. Practically, this means that a true particle size cannot be determined,

https://doi.org/10.1021/acsestair.5c00307
ACS EST Air XXXX, XXX, XXX−XXX

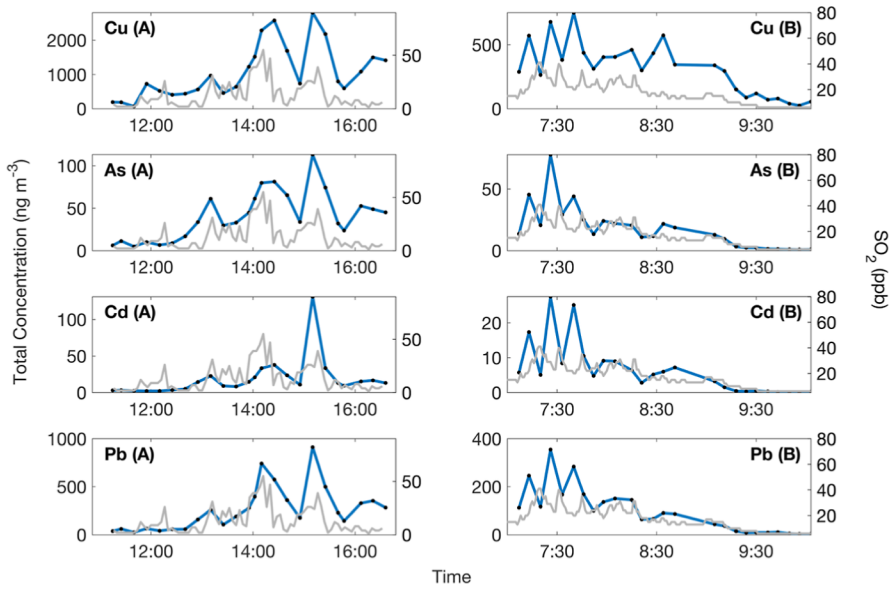

Figure 2. Time-resolved total metal(loid) concentrations (blue) for Cu, As, Cd, and Pb (determined from bulk analysis of acidified samples), and SO_2 concentrations (gray). Time-series A was collected at the University of Abitibi-Témiscamingue (500 m from the smelter entrance) and is plotted on the left-hand column. Time-series B was collected at the entrance to the smelter complex and is plotted in the right-hand column. SO_2 data from station P4 (South) are plotted for time series A, and data from the monitoring station are used for time series B. These SO_2 observations exhibited the best relationship with the elemental concentrations.

only the combined mass of the elements detected in a particle. Despite this, the particles measured by spICP-MS are considered "sub-micron" for 2 reasons. Using hypothetical mineral formulas for the major particle types, calculated diameters were almost exclusively <1 μm (Figure S1). Second, larger particles exhibit much lower transport efficiencies into the plasma, reducing the likelihood of measuring particles >1 μm.[14] While some micron sized particles were certainly analyzed, among the 1.3 million particles detected in the study, we estimate that they account for <0.2% of all particles (Figure S1). This implies that only a subset of the sampled particles are measured by spICP-ToF-MS, as further demonstrated by the greater bulk concentrations relative to the particle mass concentrations.

Finally, a limitation of the coupling of the water-based sampling with the spICP-ToF-MS analysis is that soluble particles can dissolve prior to analysis. Dissolution would be especially relevant for sulfates as well as arsenic trioxides and pentoxides, all of which are likely to be observed in this environment.[15] Dissolved elemental species are measured by the ToF-MS as a baseline signal, which was quantified using calibration standards and then converted to ng m^{-3}. Practically, this results in an underreporting of particle number concentrations.

3. RESULTS AND DISCUSSION

3.1. Time-Resolved Sampling Reveals Transient Emissions

Time-resolved total elemental concentrations of Cu, As, Cd, and Pb determined from acidified samples are presented in Figure 2 for measurement series A (left) and B (right).

Analysis of time-resolved samples revealed that atmospheric metal(loid) concentrations downwind of the smelter were highly variable, with orders of magnitude changes occurring over very short time scales. In sample set A, As, Cd and Pb concentrations (Figure 2, left column) were characterized by a baseline period of relatively low metal(loid) concentrations, followed by a prolonged period of emission, with three separate peaks of the elemental concentrations. Pb and Cd exhibited the sharpest rise in metal(loid) concentrations, occurring between 14:55 and 15:10, with a concurrent increase in many other chalcophile (sulfide-associated) elements. Cd increased 13-fold in this time period (from 10 ng m^{-3} to 131 ng m^{-3}), while Pb increased 7-fold (175−912 ng m^{-3}). Full concentration data are provided in Tables S2−S4. For the time series A data, our sampling period ended while metal(loid) concentrations were still elevated, thus we could not determine when or if they returned to the baseline values seen at the beginning of the sampling period.

During the sampling period, visible emissions were observed from the main stack of the smelter. While purely qualitative, a large visible emission event was observed to start shortly before 14:00, corresponding to the beginning of the second emission peak seen in Figure 2. It is noteworthy that our sampling location was probably too close to the smelter stack to be influenced by the plume at the height we sampled, but it is probable that visible emissions from the stack were related to fugitive emissions from elsewhere within the facility (e.g., exhaust vents).

Sample set B (Figure 2 right-hand column) was characterized by elevated airborne metal(loid) concentrations at the start of the sampling period, gradually falling over 3 h to an apparent baseline for the last three samples. Metal(loid) concentrations during the final hour of set B were within the ranges measured at the most distal upwind sites in the distance series (described below, Tables S2−S3 for concentrations). This may indicate that in the absence of transient emission events, metal(loid) concentrations downwind of the smelter are not elevated, at least for the environmental conditions present on the day of sampling. Differences in measured concentrations between the two sample sets could be attributed to differences in the environmental conditions on each sampling day. Set A was collected on a partly cloudy day with strong wind gusts, while set B was collected in dense fog and light wind, with approximately 5 cm of snow on the ground. The temperature, solar radiation, and cloud cover can significantly impact the stability of the atmosphere and thus the dispersion and dilution of a plume from a point source.[16] However, the specific processes occurring inside the smelter (e.g., reactor loading, vessel transfer, slag or matte tap) during

https://doi.org/10.1021/acsestair.5c00307
ACS EST Air XXXX, XXX, XXX−XXX

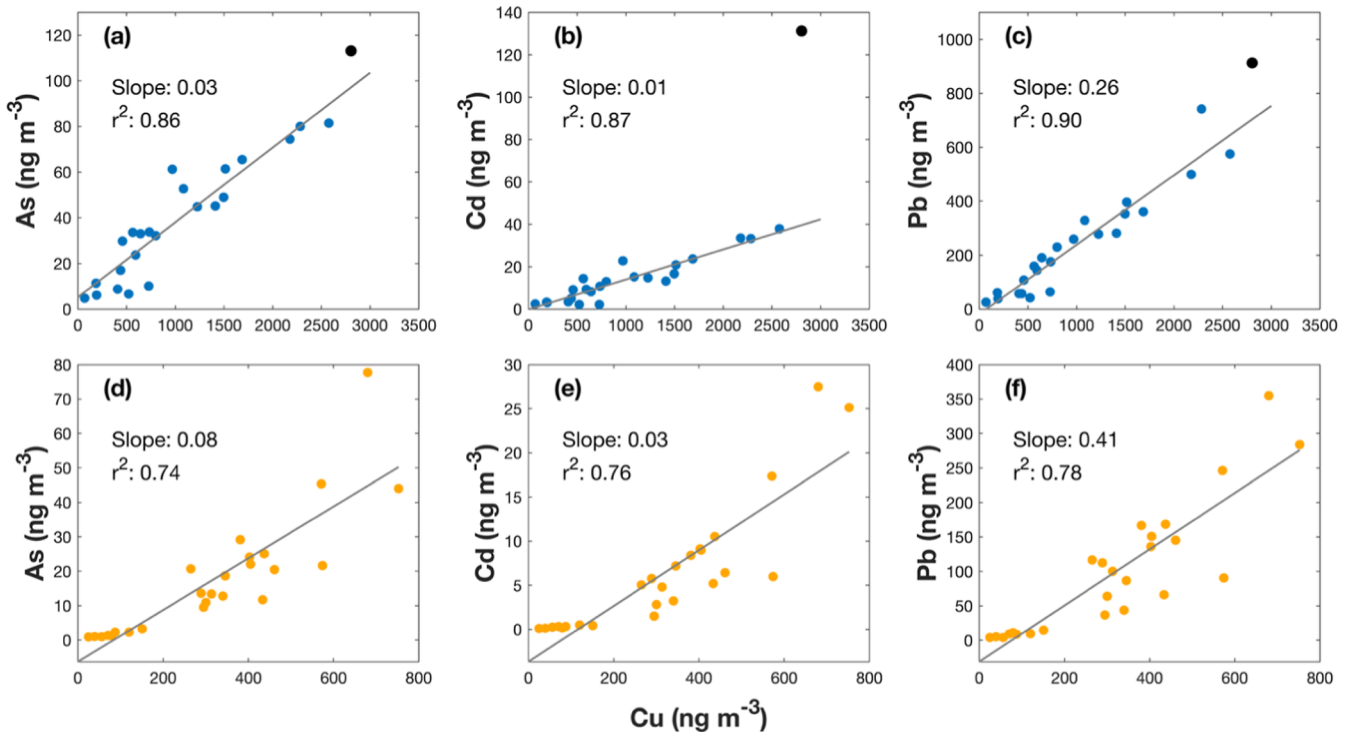

Figure 3. Correlations between total Cu and Cd, Pb and As for sample sets A (a–c) and B (d–f). Sample A-18 is plotted as a black circle in a–c, as it was a clear outlier for some elements and thus was removed when calculating correlations.

these periods are also unknown, and as such it is not possible to unambiguously determine the reason for the different behaviors between the two sample sets. Like set A, the sample location for set B was also very close to the smelter stack (~400 m) and it may have been underneath the plume. Measured emissions are likely to have originated from elsewhere in the complex (vents, etc.).

For both time series, airborne SO_2 concentrations appear to track with the measured elemental concentrations. The alignment of the SO_2 and metal(loid) time series, especially for the more volatile metal(loid)s including Cd and As, indicate that the oxidation of sulfide minerals during smelting may be responsible for the emissions. Nonetheless, SO_2 could also originate from elsewhere in the plant, such as the sulfuric acid recovery systems that follow the smelting process. In Figure 2, data from two different SO_2 monitors are used; there are multiple SO_2 monitors in the city and not all correlated with the Coriolis data described in this section, which is expected given the proximity of the measurements to a strong point source (the smelter) and corresponding large spatial gradients in concentrations.

Correlations between Cu and the three most potentially harmful metal(loid)s (Pb, As, and Cd) were examined for the acidified Coriolis-ICP-MS samples for sample sets A (Figure 3a–c) and B (Figure 3d–f). With the exception of a single high-Cd outlier (sample A18 which was also elevated in Bi, In, and Tl, Figure S2), Cu concentrations displayed strong correlations with Cd, Pb, and As concentrations (r^2 ranging from 0.76 to 0.90). From the bulk data, it is not possible to determine whether the outlier resulted from a single large particle that dominated the mass concentration. However, A18 was also an outlier for each of these elements with respect to PNC (see subsequent section), suggesting it was likely a representative sample. Nonetheless, as it is only a single sample, it is important not to overinterpret the result. Additional strong correlations among elements that are hypothesized to originate from smelting (Tl, In, Bi) are presented in Figure S2. While strong correlations were seen for both sample sets, the slopes of the best-fit lines are different. This is unsurprising, as the sets were collected at different times and it may simply reflect different compositions of the feedstock.

Elemental concentrations reported by the Xact XRF instrument for this time frame at the monitoring station are presented in Figures S3–S5 and compared to the Coriolis-ICP–MS results. Notably, extremely poor correlations were observed between Cu and As, Pb or Cd when using the XRF data. Additionally, the XRF detected a maximum of 11 ng m^{-3} of Cd during the sampling period, while levels as high as 131 ng m^{-3} were measured by Coriolis-ICP–MS. These elevated Cd concentrations were detected over short time scales using the Coriolis, while the XRF instrument measures an average hourly concentration. The data presented in Figures 2 and 3 suggest that the Coriolis-ICP–MS method is better for resolving dynamic elemental concentrations of airborne particles, providing new insights into the duration of transient emissions and the metal(loids) associated with such events.

3.2. Transect-Sampling Demonstrates the Downwind Persistence of Smelter Emissions

A set of 30 air samples were collected at 12 locations along a distance transect over a period of 7 h, with 2 samples collected at each location. In addition, while sampling the closest downwind site, a large visible emission event of approximately 30 min occurred (Figure S6), and so sampling was increased to 8 times over a period of roughly 1 h. The average concentrations of Si, Fe, Cu, As, Cd, and Pb are presented for each sampling location in Figure 4a.

https://doi.org/10.1021/acsestair.5c00307
ACS EST Air XXXX, XXX, XXX–XXX

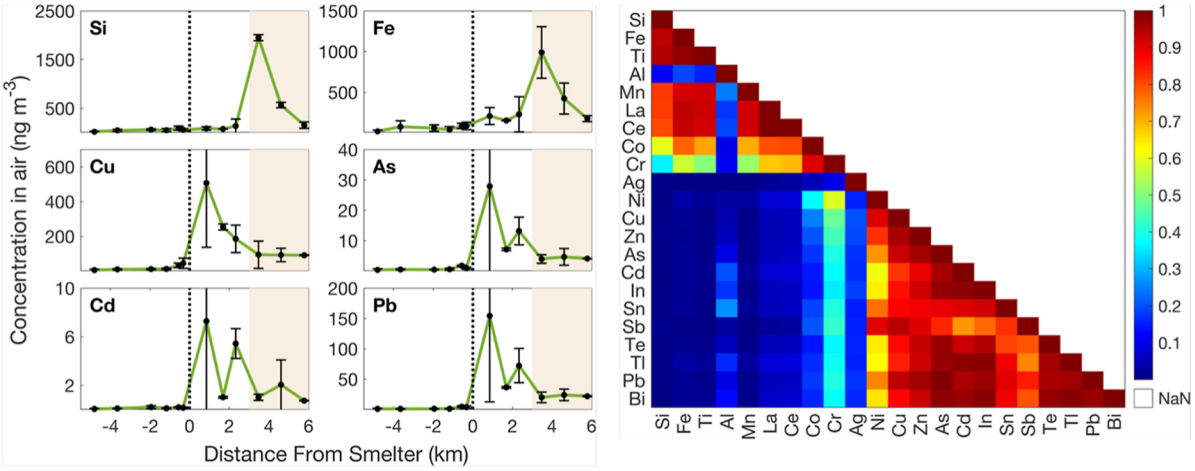

Figure 4. A) Total concentrations of Si, Fe, Cu, As, Cd, and Pb (determined in acidified samples) in air sampled along a distance transect upwind and downwind of the smelter. Each point represents the average and standard deviation for 2 samples except for the closest downwind site where 8 samples were collected and averaged. The black dotted line represents the location of the smelter; negative values are upwind, positive values are downwind. The shaded area indicates samples that were collected along an unpaved road. (B) Correlation heatmap of total elemental concentrations across the distance-transect sample set.

Upwind of the smelter complex, the concentration of potentially toxic elements, including As, Cd, and Pb were low, generally between 0.1 and 5 ng m^{-3}, and did not show a large increase between 4.5 km (most distal sample) and 1.8 km upwind. Pb, As, and Cu concentrations did increase at the two upwind samples closest to the smelter (0.5 and 0.3 km upwind), but concentrations still remained relatively low. By contrast, downwind of the smelter, concentrations for Cu, Cd, As, and Pb all increased by 1−2 orders of magnitude when compared to the upwind levels (Figure 4). During the visible transient emission event, measured average concentrations were initially low, however, they then spiked and subsequently subsided over a period of roughly 30 min (Figure S7). This observation reinforces the utility of acquiring high frequency data.

Airborne metal(loid) concentrations of Cu, As, Cd, Pb and several other elements of concern were elevated at all downwind sites, relative to their upwind concentrations. In fact, their concentrations did not show any substantial decrease over the 3 most distal sites (Table S3), suggesting that the range of elevated concentrations could extend beyond the ∼6 km sampled. While previous studies have identified that a much larger area (>100 km radius) surrounding the smelter is impacted by its emission, those conclusions were based on the measurements of soils, sediments, snow, or biota, all of which accumulate metal(loid)s over time, and cannot provide information on real-time emissions.[15,17−19] A better understanding of the specific sources of the emissions, and their impact on human health will require a comprehensive sampling of airborne metal(loid) concentrations over space and time, taking weather and specific smelting activities into account. The strategy shown here closes this gap, with the ability to rapidly sample air with a portable device in order to obtain precise elemental concentrations with low detection limits. While the distance transect illustrates the downwind persistence of airborne metal(loid) concentrations, interpretation is limited by the use of a single sampling device since concentrations vary both spatially and temporally. Although the meteorological conditions (wind speed and direction) remained constant throughout the sampling period, we cannot determine whether upwind concentrations would have been impacted by the emission event, although it would be highly unlikely. Ongoing distance-resolved studies are being performed with multiple sampling devices to allow for a better understanding of the transport of metal(loid)s from the smelter.

Fe, Si, and other lithophile elemental concentrations did not display the same orders-of-magnitude increase immediately downwind of the smelter. However, at 3 km downwind, their concentrations increased significantly, corresponding to the samples that were collected along an unpaved road. Vehicles periodically passed the sampling locations, suspending mineral dust from the road that was then captured. Although the objective was to sample the impact of the smelter over a range of distances, the capture of suspended dust from the road offers further evidence that (a) airborne chalcophile elements are derived from the smelter, and (b) that the elemental concentrations from the air samples reflected well the environment from which they were sampled. Despite a large increase in particles sampled at the three most distal locations due to the unpaved road, concentrations of chalcophiles did not increase, suggesting they were not present at appreciable levels in the mineral dusts suspended from the road.

The correlations of airborne metal(loids) observed along the distance transect are illustrated in Figure 4B. The correlation heatmap clearly displays two groups of elements that showed strong correlations within the groups, but only very limited correlation between groups. These elements generally align with the Goldschmidt classification of lithophiles (elements that comprise silicate minerals and are likely suspended from the dirt road, i.e. local mineral dusts) and chalcophiles (elements that are associated with sulfide minerals, and which can likely be attributed to the smelting emissions).[20]

3.3. spICP-ToF-MS Signatures Indicate Possible Sources of Contaminants

Source apportionment of PM can be performed using bulk concentrations, including statistical approaches such as positive matrix factorization (PMF).[21] However, bulk analyses do not allow differentiation between externally and internally mixed metal(loid)s in airborne particles, which limits their ability to distinguish sources that are close to each other or exhibit

https://doi.org/10.1021/acsestair.5c00307
ACS EST Air XXXX, XXX, XXX−XXX

similar temporal variability. By determining the composition of individual particles using spICP-ToF-MS, it is possible to gain more precise insights into the emission sources.

For simplicity, particles can be broadly classified as originating from smelting, or feedstock handling (trucking and unloading of concentrates and feedstock from recycled electronics). Given the limited number of days of sampling and the upper size-limit of the spICP-MS analysis ($\sim\leq$ 1 μm particle diameters), any assignment of particle sources described herein is only a preliminary assessment; future sampling of additional locations and sample types is needed.

Across the three sample sets (A, B, D) considered here, 1,339,914 particles were measured, each with data for 25 isotopes. This resulted in tens of thousands of unique elemental signatures and thus, it is impractical to provide a description of every particle signature that was measured. Rather, the major particle types are first described, followed by a detailed analysis of Pb- and As-bearing particles, as these are two of the most concerning contaminants that are present near the site of the smelter. spICP-ToF-MS summary data for each sample are included in Tables S5–S7 and visualized in Figure S8.

All samples were dominated by Fe-containing particles, followed by Al- and Si-bearing particles. More than 90% of all particles contained some combination of these three elements. This is expected, because Fe is likely associated with every possible source of PM including mineral dust aerosols (MDA), copper concentrate, slag, and condensates. Al and Si are associated with MDA and slag and could also be present in the feedstock, although likely at low concentrations. Chalcophile-bearing particles were abundant in all samples downwind of the smelter, accounting for about 20% of the particles (Figure S8). Cu was the most abundant chalcophile element (average downwind = PNC 2.11 × 10^6 m^{-3}) with Zn, Pb, Ag, Bi, As, Sn, Sb and In also detected in all downwind samples (ranging from 1.62 × 10^5 (Sb) to 1.70 × 10^6 particles m^{-3} (Bi)). In contrast, samples collected >1 km upwind of the smelter contained very few chalcophile particles, accounting for <1% of the total particle number. Cu was the most abundant chalcophile element in the upwind particles (7.29 × 10^4 m^{-3}), with smaller numbers of detected Zn (1.40 × 10^4 m^{-3}), Sn (1.83 × 10^4 m^{-3}) and Pb (2.74 × 10^4 m^{-3}) particles. These particles could originate from regional mining operations, or other anthropogenic sources, including vehicle emissions. There were no As or In particles detected in the upwind samples >1 km from the smelter.

For time series A, strong correlations were observed for PNC between Cu and trace elements, including As, Cd, Pb, Sb, In, and Bi (Figure S9). Not only are these correlations consistent with what was observed in the bulk measurements (Figure 3), but the outlier sample (A18) was also anomalous with respect to PNC for many elements. The similar correlations observed for both PNC and the total concentration likely indicate that the subset of particles analyzed by spICP-ToF-MS was consistent across the samples.

To investigate the sources of particles based on their multielement composition, As- and Pb-bearing particles that were collected at 0.5 km from the smelter stack (series A) were investigated further. This data set is most useful for source apportionment, as time was the only variable (as opposed to the distance transect). Furthermore, multiple transient emission spikes were measured, as opposed to the single emission event in series B. Particle number concentrations (PNCs) for As and Pb are presented in Figure 5a, with their major elemental associations given in 5b (As) and 5c (Pb). For

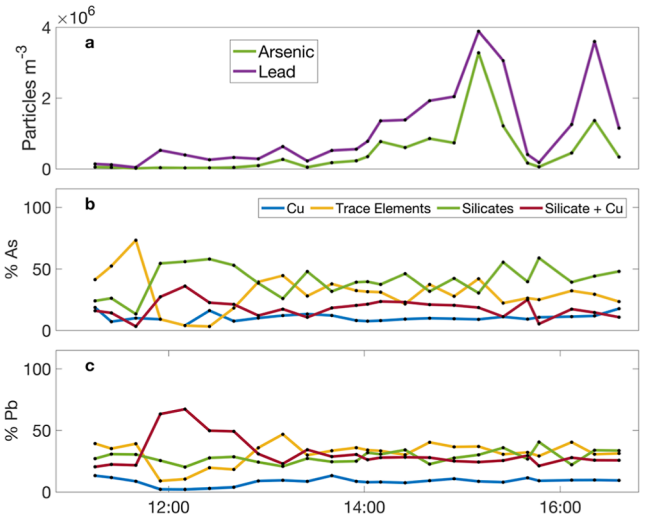

Figure 5. a) Time-resolved particle number concentration of arsenic- and lead-bearing submicron particles measured by spICP-TOF-MS during series A for samples taken at 0.5 km from the smelter stack. (b) Time-resolved classification of As-bearing particles based upon the major coconstituent elements/element groupings: (i) Cu; (ii) trace elements, but no Cu/Al/Si, (iii) Al–Si (silicate) and (iv) Cu–Al–Si (silicate + Cu). (c) The same classification as B, but for Pb-bearing particles.

5b and 5c, the Pb and As particles are classified with respect to elements, or groups of elements that co-occur with Pb or As in the particles, and the fraction (by number) of each association with Pb/As is plotted with respect to time. If Pb or As occurred with Al and Si, but not Cu, they were classified as silicate associated (regardless of whether they contained other elements). If Pb/As were found with Cu, but not with Al or Si, they were classified as Cu associated, again regardless of the other elements present. If Pb or As occurred either alone, or only with other trace elements (e.g., Bi, Sb, In, Sn), they were classified as trace-element associated. These simple groups were created to assess whether there were any major changes to the elemental associations of Pb and/or As over time.

Over the 5 h time series, the As and Pb PNCs varied significantly, with an initial 2 h period of relatively low concentrations, followed by two clear peaks occurring at 15:10 and 16:20, respectively (Figure 5a). The Pb and As PNCs increased by 20- and 66-fold, respectively, during the first peak. In stark contrast, there were few clear trends for the distribution of Pb and As among different particle types. Indeed, the only observable trend occurred during the first 2 h of the time series, when PNCs were relatively low, and where there was a short-lived increase in the fraction of Pb and As associated with Al/Si, in addition to a corresponding decrease in the fraction of Pb and As that were associated with the trace elements. For both As and Pb, the smallest fraction was the Cu-associated particles across the series, with greater proportions of the elements occurring with silicates, silicates plus Cu, and trace elements.

A large change in PNC without any corresponding shift in the major particle associations indicates a single source is likely responsible for the majority of the measured particles. The elemental associations and mobilization mechanism of the two

https://doi.org/10.1021/acsestair.5c00307
ACS EST Air XXXX, XXX, XXX–XXX

main emission sources (smelting and feedstock handling) are very likely to be different from one another, specifically with regard to trace element co-occurrence, as described below. Thus, if both sources contributed to the observed transient spike in PNC (Figure 5a), a measurable shift in the particle classification would likely have been observed, but was not (Figure 5b,c). There are several additional lines of evidence supporting this observation. As and Pb particles associated with the feedstock (Cu ore minerals) likely (a) contain Cu, and (b) do not contain Al/Si. The fact that fewer than 15% of the As and Pb particles reflect this composition (and that this fraction remains stable throughout the time series) indicates that suspended copper concentrates do not account for the majority of the measured As and Pb particles. Thus, the major element classification suggests that most particles measured during sample set A may originate from fugitive smelting emissions (i.e., from vents of the smelter building).

The relationships of As and Pb with other trace elements provided the greatest insight into the possible sources of emission. In this case, Sn, In, Sb, and Bi were considered given that (i) they were detected in large numbers, ranging from 4,070 for Sb (2.5×10^5 m^{-3}) to 49,599 for Bi (2.85×10^6 m^{-3}), (ii) they coexisted with As and/or Pb in many particles, and (iii) they are associated with specific components of the smelting feedstock. The multielement compositions were used as an indicator of particle source based on the origins of the trace elements. As, Bi, and Sb are common components of Cu ore, and are often found together with Cu in minerals such as tennantite, enargite, and tetrahedrite.[22,23] By contrast, Sn and In do not commonly occur in Cu ore, and when they do co-occur in the same deposits (in some rare granite-related deposits and polymetallic skarns), they are not found in Cu minerals.[24] Rather, Sn and In are very likely to be present in recycled copper, as both are components of solder and waste electronics including indium–tin oxides (ITOs) in screens.[25,26] Commercial uses of As are extremely limited, making it unlikely to occur in recycled copper streams. Similarly, Bi and Sb are used in some limited applications including specialized solders and some electronics, but largely they are not expected to be part of the recycling stream.[26] Pb is unique among these 6 elements in that it is common in both recycling (leaded solders) and Cu ore. Particles were therefore assigned to a source based upon coexistence of these trace elements in single particles. If a single particle contained elements associated with ore (As/Sb/Bi) together with those associated with recycling (In/Sn), then the particle likely originated from the smelting process since these two feedstocks are combined in the smelter's reactor. Particles containing Cu together with As/Sb/Bi (but not In/Sn) were classified as ore minerals, and particles with Cu together with Sn/In (but not As/Sb/Bi) were classified as recycled material; particles of both ore minerals and recycled material could have been mobilized by feedstock handling or storage. This classification scheme is illustrated in Figure 6a. Confidence in the smelting origin is greater for single particles that contain greater numbers of trace elements; As, Sb, and In contained the greatest number of co-occurring trace elements, with Pb, Sn, and Bi comparatively fewer (Figure S10). Figure 6b presents the distribution of each trace element based upon the number of particles in each classification. For all 6 examined trace elements, the majority of particles that could be classified were determined to originate from the smelting process, ranging from 68% (Bi) to

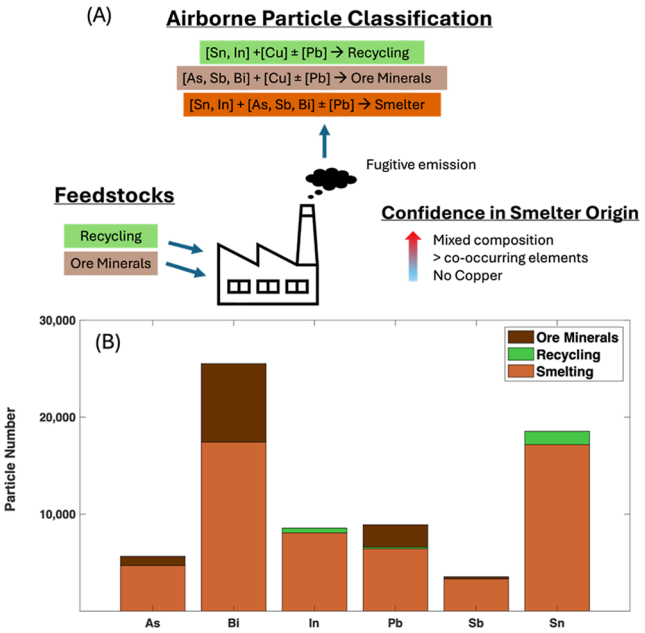

Figure 6. a) Classification scheme for airborne particles based on their trace element content and measured by spICP-ToF-MS for time series A. (b) Trace element-bearing particles classified as having a feedstock origin (ore minerals or recycling), or a smelting origin. Note that (b) refers only to the particles that could be classified (see Table S11 for full results).

94% (In). The same results as a function of particle mass are presented in Figure S11.

In some particles, too few elements were measured to allow classification. For example, an As–Bi particle without Cu or other trace elements cannot be classified as an ore mineral (as it does not contain Cu), but neither can it be classified as having a smelting origin, as it does not contain Sn or In. Despite this limitation, most of the trace element-bearing particles could be classified, except for Sn (57% unclassified, Table 2). The classification scheme was particularly successful

Table 2. Percentage of Trace Element-Bearing Particles Belonging to Each Particle Class as Defined in Figure 6.[a]

	% of particles			
	smelter	recycling	ore	unclassified
Sn	39	3	N/A	57
In	76	5	N/A	20
As	65	N/A	13	21
Sb	82	N/A	6	13
Bi	35	N/A	16	49
Pb	33	1	26	40

[a]N/A is indicated for the elements where the given element was used to identify a particle type.

for In, As and Sb, where ≥80% of particles could be classified. Importantly, the results were not biased by the mass of the particles (i.e., where large particles containing systematically more elements were classified with a "smelting" origin). Figure S12 demonstrates that there was no significant difference in the mass of each trace element classified as an ore mineral, or a smelting-derived particle.

To further interrogate the data at the single-particle level, heatmaps were generated for the 20 most common As (Figure

https://doi.org/10.1021/acsestair.5c00307
ACS EST Air XXXX, XXX, XXX–XXX

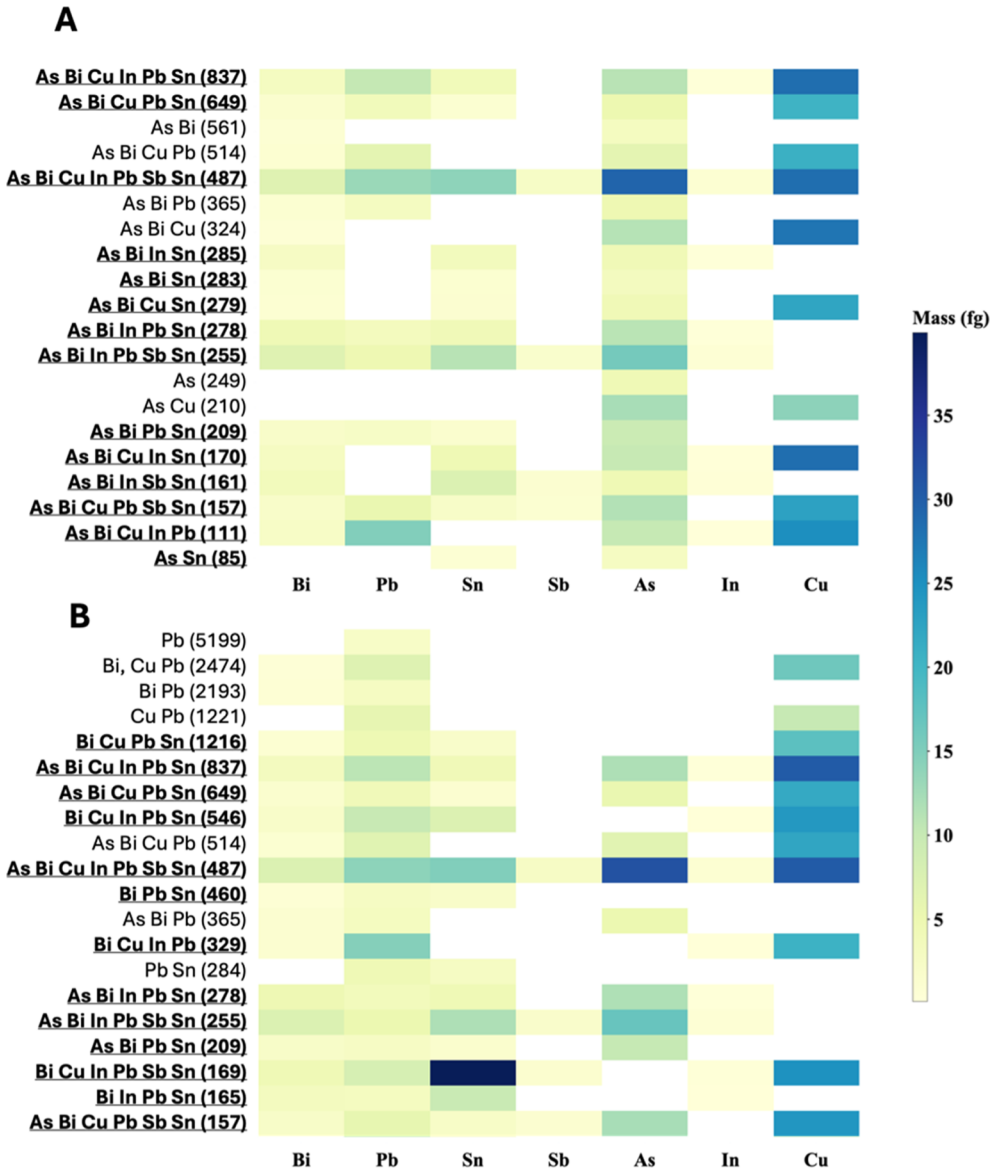

Figure 7. Heatmaps displaying the 20 most frequent combinations of (A) As and (B) Pb particles, classified based on their co-occurrence with Cu and other trace elements (Bi, Sn, Sb, In). The color corresponds to the average mass of each element in each particle class (in femtograms, fg). The number of particles in parentheses represents the total number of that combination detected across the 24 samples in series A. Note that the major elements (Fe, Al, Si, etc.) are not considered in this figure, though they were present in many of the particles. Underlined particle compositions, containing both trace element groups (As/Sb/Bi and Sn/In), have been classified as smelter-derived, as described in the text. The 20 lines of heat map accounted for 90% of the total number of As particles and 83% of the Pb particles.

7A) and Pb (Figure 7B) containing particles which also contained the trace elements used for classification: (Sb, Bi, Sn, In) and/or Cu. In the heatmap of the major As and Pb particle types, those that have been attributed to the smelting process have been underlined. Groups not underlined include those classified as ore minerals, recycling (only for Pb) and unclassified.

It is noteworthy that Cu was not present in many of these particle types, especially for As (46% of all As-containing particles did not contain Cu). Although it is difficult to determine whether an element is truly absent from a particle in spICP-ToF-MS (or simply present in small amounts below the detection limit), when Cu is present, it is a major component of the particles, with a much greater mass than the trace elements considered (darker colors on the heatmap in Figure 7). Thus, the absence of Cu in these particle types is unlikely to be an artifact. Moreover, the sensitivity of Cu was 8× that of As, increasing our confidence in the true lack of Cu in these particles. Because Cu is separated from trace elements during the smelting process, a particle with multiple trace elements but no Cu likely originates from smelting. The value of the multielement capability of spICP-ToF-MS is highlighted here. Based upon the strong PNC correlations between As and Cu that are shown in Figure S9, one might falsely conclude that mineral particles were the primary source of As particles. Based upon the heatmap, this clearly is not the case.

The analysis of multielement compositions at the single particle level using spICP-ToF-MS clearly provides information that cannot be obtained from bulk-scale analyses. For example, strong correlations were seen between bulk concentrations and PNCs of Cu and As/Pb in Figures 3 and S9, respectively, which could be interpreted as As, Pb, and Cu

https://doi.org/10.1021/acsestair.5c00307
ACS EST Air XXXX, XXX, XXX−XXX

being present together in particulate emissions. However, at the single particle level, nearly half of all As-bearing particles did not contain Cu. Furthermore, it is difficult to use trace elements for source apportionment from bulk data alone. Single particle data reveals diverse groups of trace elements in individual particles, likely fingerprinting a smelting origin. While there are multiple lines of evidence supporting the smelting origin of the measured particles, linking these single particle data to the total elemental concentrations is nonetheless tenuous. If, for example, particles >1 μm primarily originated from concentrate handling, then the source apportionment based on spICP-ToF-MS data would be incomplete.

This study presents several advancements in airborne PM analysis, providing new insights into emissions from copper smelting. Specifically, the Coriolis-μ air sampler is a highly effective tool for temporally and spatially resolved elemental analysis in air. Its capability surpasses the time resolution even of specialized instruments such as the Xact XRF instrument, while enabling the precise quantification and low detection limits of an ICP−MS. Furthermore, the use of this device in concert with spICP-ToF-MS provided a much deeper understanding of the emission sources as compared to bulk elemental concentrations alone. Across the 80 samples collected, we measured the compositions of 1.3 million individual particles, providing a large data set for multielement particle analysis.

The main limitations in this study were the use of a single sampling device, and limited environments sampled (only outside the smelter complex). Future work will employ multiple samplers in order to determine metal(loid) concentrations at multiple points simultaneously, with downwind transport further constrained. Methodological limitations include uncertainties in the particle sizes sampled and analyzed, and issues with particle solubility (for spICP-ToF-MS) or lack of solubility (for total analysis). Ongoing work utilizes SEM to compliment the spICP-ToF-MS results. Method optimization is ongoing and will continue to open new research avenues for this emerging technique.

■ ASSOCIATED CONTENT

Data Availability Statement

Data is available in the Supporting Information, including additional figures, tables, and data summary. A link to the raw spICP-TOFMS data set is included.

Supporting Information

The Supporting Information is available free of charge at https://pubs.acs.org/doi/10.1021/acsestair.5c00307.

(PDF)

■ AUTHOR INFORMATION

Corresponding Authors

Aaron J. Goodman − *Département de Chimie, Université de Montréal, Montréal H2 V0B3, Canada;* orcid.org/0000-0003-3704-7454; Email: agoodman@mines.edu

Kevin J. Wilkinson − *Département de Chimie, Université de Montréal, Montréal H2 V0B3, Canada;* orcid.org/0000-0002-7182-3624; Email: kj.wilkinson@umontreal.ca

Authors

Houssame-Eddine Ahabchane − *Département de Chimie, Université de Montréal, Montréal H2 V0B3, Canada*

Patrick L. Hayes − *Département de Chimie, Université de Montréal, Montréal H2 V0B3, Canada*

Complete contact information is available at: https://pubs.acs.org/10.1021/acsestair.5c00307

Notes

The authors declare no competing financial interest.

■ ACKNOWLEDGMENTS

The authors acknowledge funding from Fonds de recherche du Québec—Nature et technologies (FRQNT), EcoToQ, Canada Foundation for Innovation and Glencore. We thank Daniel Proulx and the ONICSE organization for providing access to some of the sampling locations. We thank Glencore for providing XRF data and insight into some of the source materials.

■ REFERENCES

(1) Lu, Y.; Bai, X.; Fu, Z.; Yang, J.; Zhou, Y.; Liu, W.; Hao, Y.; Zhao, H.; Tian, H. Atmospheric Emission Inventory of Trace Elements from Non-Ferrous Metal Smelting Industries in China. *Resour Conserv Recycl* **2026**, *225*, 108627.

(2) Pacyna, J. M.; Pacyna, E. G. An Assessment of Global and Regional Emissions of Trace Metals to the Atmosphere from Anthropogenic Sources Worldwide. *Environ. Rev.* **2001**, *9* (4), 269−298.

(3) Savard, M. M.; Bonham-Carter, G. F.; Banic, C. M. A Geoscientific Perspective on Airborne Smelter Emissions of Metals in the Environment: An Overview. *Geochem. Explor. Environ. Anal.* **2006**, *6* (6), 99−109.

(4) Schipper, B. W.; Lin, H. C.; Meloni, M. A.; Wansleeben, K.; Heijungs, R.; van der Voet, E. Estimating Global Copper Demand until 2100 with Regression and Stock Dynamics. *Resour Conserv Recycl* **2018**, *132*, 28−36.

(5) Northey, S.; Mohr, S.; Mudd, G. M.; Weng, Z.; Giurco, D. Modelling Future Copper Ore Grade Decline Based on a Detailed Assessment of Copper Resources and Mining. *Resour Conserv Recycl* **2014**, *83*, 190−201.

(6) Nemmar, A.; Holme, J. A.; Rosas, I.; Schwarze, P. E.; Alfaro-Moreno, E. Recent Advances in Particulate Matter and Nanoparticle Toxicology: A Review of the in Vivo and in Vitro Studies. *BioMed Res. Int.* **2013**, *2013*, 1.

(7) Tardif, Y.; Richard, L.; Bellamy, D.; Ahabchane, H. E.; Tharaud, M.; Schlatt, L.; Dourlent, A.; Trieu, N.; King, J.; Wilkinson, K. J.; Hayes, P. L. Contrasting the Elemental Composition of Fine Particulate Matter in Urban and Remote Samples Using Single Particle Inductively Coupled Plasma Time-of-Flight Mass Spectrometry (SP ICP-ToF-MS). *Aerosol Sci. Technol.* **2025**, *59* (9), 1065−1081.

(8) Torregrosa, D.; Grindlay, G.; de la Guardia, M.; Gras, L.; Mora, J. Determination of Metallic Nanoparticles in Air Filters by Means Single Particle Inductively Coupled Plasma Mass Spectrometry. *Talanta* **2023**, *252*, 123818.

(9) Wolk, C. Invisible Damage, Imaginary Injuries, and the Political Ecology of Redress in a Quebec Mining and Smelter Town. Thesis, University of Delaware, 2023.

(10) Lockwood, T. E.; Gonzalez de Vega, R.; Du, Z.; Schlatt, L.; Xu, X.; Clases, D. Strategies to Enhance Figures of Merit in ICP-ToF-MS. *J. Anal. At. Spectrom.* **2024**, *39* (1), 227−234.

(11) Pace, H.; Rogers, N.; Jarolimek, C.; Coleman, V.; Higgins, C.; Ranville, J. Determining Transport Efficiency for the Purpose of Counting and Sizing Nanoparticles via Single Particle Inductively

Coupled Plasma Mass Spectrometry. *Anal. Chem.* **2011**, *83* (24), 9361−9369.
(12) Lockwood, T. E.; Schlatt, L.; Clases, D. SPCal − an Open Source, Easy-to-Use Processing Platform for ICP-TOFMS-Based Single Event Data. *J. Anal. At. Spectrom.* **2025**, *40* (1), 130−136.
(13) Carvalho, E.; Sindt, C.; Verdier, A.; Galan, C.; O'Donoghue, L.; Parks, S.; Thibaudon, M. Performance of the Coriolis Air Sampler, a High-Volume Aerosol-Collection System for Quantification of Airborne Spores and Pollen Grains. *Aerobiologia* **2008**, *24* (4), 191−201.
(14) Lomax-Vogt, M.; Carter, L. M.; Wielinski, J.; Kutuzov, S.; Lowry, G. V.; Sullivan, R.; Gabrielli, P.; Olesik, J. W. Challenges in Measuring Nanoparticles and Microparticles by Single Particle ICP-QMS and ICP-TOFMS: Size-Dependent Transport Efficiency and Limited Linear Dynamic Range. *J. Anal. At. Spectrom.* **2025**, *40*, 848.
(15) Telmer, K.; Bonham-Carter, G. F.; Kliza, D. A.; Hall, G. E. M. The Atmospheric Transport and Deposition of Smelter Emissions: Evidence from the Multi-Element Geochemistry of Snow, Quebec, Canada. *Geochim. Cosmochim. Acta* **2004**, *68* (14), 2961−2980.
(16) Dubey, R. R.; Mahato, B.; Yaghoobian, N. Effect of the Atmospheric Stability Condition on Buoyant Plume Dynamics. *Phys. Fluids* **2024**, *36* (12), 126615.
(17) Telmer, K. H.; Daneshfar, B.; Sanborn, M. S.; Kliza-Petelle, D.; Rancourt, D. G. The Role of Smelter Emissions and Element Remobilization in the Sediment Chemistry of 99 Lakes around the Horne Smelter, Québec; **2006**; Vol. *6*, 187, 202, .
(18) Zdanowicz, C. M.; Banic, C. M.; Paktunc, D. A.; Kliza-Petelle, D. A. Metal Emissions from a Cu Smelter, Rouyn-Noranda, Québec: Characterization of Particles Sampled in Air and Snow. *Geochem. Explor. Environ. Anal.* **2006**, *6* (2−3), 147−162.
(19) Savard, M. M.; Bégin, C.; Parent, M.; Marion, J.; Smirnoff, A. Dendrogeochemical Distinction between Geogenic and Anthropogenic Emissions of Metals and Gases near a Copper Smelter. *Geochem. Explor. Environ. Anal.* **2006**, 237−247.
(20) Goldschmidt, V. M. Geochemistry. *Soil Sci.* **1954**, *78*, 156.
(21) Fakhri, N.; Stevens, R.; Downey, A.; Oikonomou, K.; Sciare, J.; Afif, C.; Hayes, P. L. Source Apportionment of PM2.5 in Montréal, Canada, and Health Risk Assessment for Potentially Toxic Elements. *Atmos. Chem. Phys.* **2024**, *24* (2), 1193−1212.
(22) George, L. L.; Cook, N. J.; Ciobanu, C. L. Minor and Trace Elements in Natural Tetrahedrite-Tennantite: Effects on Element Partitioning among Base Metal Sulphides. *Minerals* **2017**, *7* (2), 17.
(23) Delbeke, K. *Copper Concentrates Environmental and Human Health Hazard Classification*; 2014.
(24) Werner, T. T.; Mudd, G. M.; Jowitt, S. M. The World's by-Product and Critical Metal Resources Part III: A Global Assessment of Indium. *Ore Geol Rev.* **2017**, *86*, 939−956.
(25) Avarmaa, K.; Taskinen, P. The Influence of Aluminum on Indium and Tin Behaviour During Secondary Copper Smelting. *Extraction*; Springer International Publishing, 2018, pp 1061−1071.
(26) Zhang, S.; Ding, Y.; Liu, B.; Chang, C. chi. Supply and Demand of Some Critical Metals and Present Status of Their Recycling in WEEE. *In Waste Manag.* **2017**, 113−127.


CAS BIOFINDER DISCOVERY PLATFORM™
BRIDGE BIOLOGY AND CHEMISTRY FOR FASTER ANSWERS
Analyze target relationships, compound effects, and disease pathways
Explore the platform
CAS
A division of the American Chemical Society

https://doi.org/10.1021/acsestair.5c00307
ACS EST Air XXXX, XXX, XXX−XXX